Phenotypic and Genetic Analysis of a Novel Rat Model for Hereditary Cataract.

A Dissertation Submitted to
the Graduate School of Life and Environmental Sciences,
the University of Tsukuba
in Partial Fulfillment of Requirements
for the Degree of Doctor of Philosophy in Science
(Doctoral Program in Biological Sciences)

Kei Watanabe

Table of Contents

Abbreviations

KFRS, Kyoto Fancy Rat Stock

B6J, C57BL/6J

Mip, major intrinsic protein of eye lens fiber

Aqp0, aquaporin 0

NBRP Rat, The National BioResource Project for the Rat in Japan

RT, room temperature

qRT-PCR, quantitative RT-PCR

Cryaa, crystallin, alpha A

Crygb, crystallin, gamma B

Crygd, crystallin, gamma D

Casp6, caspase 6

Lim2, lens intrinsic membrane protein 2

Bfsp1, beaded filament structural protein 1, in lens-CP94

Bfsp2, beaded filament structural protein 2, phakinin

Gja3, gap junction protein, alpha 3

Gja8, gap junction protein, alpha 8

aa, amino acid

CDH2, N-cadherin

CTNNB1, β-catenin

Cter , C-terminal

Nter, N-terminal

NMD, nonsense-mediated messenger RNA decay

Abstract

The Kyoto Fancy Rat Stock 4 (*kfrs4*) mutation, which causes congenital cataracts, is a recessive mutation found in the Kyoto Fancy Rat Stock (KFRS) background. Within 1 month of birth, all *kfrs4/kfrs4* homozygotes developed cataracts, with severe opacity in the nuclei of the lens. In contrast, no opacity was observed in the *kfrs4/+* heterozygotes. I continued to observe these rats until they reached 1 year of age and found that cataractogenesis did not occur in *kfrs4/+* rats. To define the histological defects in the lenses of *kfrs4* rats, sections of the eyes of these rats were prepared. Although the lenses of *kfrs4/kfrs4* homozygotes showed severely disorganized fibers and vacuolation, the lenses of *kfrs4/+* heterozygotes appeared normal and similar to those of wild-type rats. I used positional cloning to identify the *kfrs4* mutation. The mutation was mapped to an approximately 9.7-Mb region on chromosome 7, which contains the *Mip* gene. This gene is responsible for a dominant form of cataract in humans and mice. Sequence analysis of the mutant-derived *Mip* gene identified a 5-bp insertion. This insertion is predicted to inactivate the MIP protein, as it produces a frameshift that results in the synthesis of six novel amino acid residues and a truncated protein that lacks 136 amino acids in the C-terminal region, and no MIP immunoreactivity was observed in the lens fiber cells of *kfrs4/kfrs4* homozygous rats using an antibody that recognizes the C- and N-terminus of MIP. In addition, the *kfrs4/+* heterozygotes showed reduced expression of *Mip* mRNA and MIP protein and the *kfrs4/kfrs4* homozygotes showed no expression in the lens.

These results indicate that the *kfrs4* mutation conveys a loss-of-function, which leads to functional inactivation though the degradation of *Mip* mRNA by an mRNA decay mechanism.

Introduction

The most common intraocular disease in humans is cataract, a leading cause of visual impairment and blindness. This disease can be broadly divided into early-onset cataract and age-related cataract [Reddy et al. 2004]. Although early-onset cataract, including congenital cataract and juvenile cataract, is much less common than age-related cataract, it is one of the most common causes of blindness in children, with a prevalence of 1 to 6 in 10,000 live births worldwide [Reddy et al. 2004]. In addition, approximately half of all early-onset cataracts may have a genetic basis [Francis et al. 2000; Hejtmancik and Smaoui. 2003]. Therefore, the identification of the responsible genes is very important for elucidating the molecular mechanisms that underlie cataractogenesis.

Most cases of early-onset cataract are inherited as an autosomal dominant trait, but autosomal recessive and X-linked forms are also known [Francis et al. 2000; Santana and Waiswo 2011]. One of the dominant genes, major intrinsic polypeptide gene (*Mip,* also known as aquaporin 0 or *Aqp0*), has been shown to play a crucial role in the transparency and optical accommodation of the ocular lens [Chepelinsky 2009; Santana and Waiswo 2011]. MIP is the most abundant membrane protein in the lens fiber cells, constituting more than 60% of the total membrane protein content of these cells [Bloemendal et al. 1972; Gorin et al. 1984]. Several studies indicate a dual function of MIP as a water channel and a cell-to-cell adhesion molecule in the ocular lens fibres [Chepelinsky et al. 2009; Kumari et al. 2009; Varadaraj et al.

2010]. In addition to functioning as a water channel and as a cell-to-cell adhesion factor, MIP plays a structural role; it is required to maintain the transparency of the lens and the organization of the lens fibers.

Mutations in *MIP* have been identified in mutation screening supported by linkage analyses of the families, including those of patients with congenital cataract [Shiels and Bassnett. 1996; Berry et al. 2000; Geyer et al. 2006; Gu et al. 2007; Lin et al. 2007; Wang et al. 2010; Wang et al. 2011; Yang et al. 2011; Ding et al. 2014; Yu et al. 2014]. All of the characterized *Mip* mutations are associated with cataract as the dominant phenotype, which could be explained by the dominant negative and gain-of-function effect of the *Mip* mutant allele [Shiels and Bassnett. 1996; Francis et al. 2000; Varadaraj et al. 2008; Chepelinsky 2009; Kumari and Varadaraj 2009; Varadaraj et al. 2010]. *Mip* mutant mice exhibit cataract as a result of disrupted lens differentiation [Shiels and Bassnett. 1996; Shiels et al. 2001; Sidjanin et al. 2001; Al-Ghoul et al. 2003; Okamura et al. 2003]. These pathological observations suggest that MIP has essential roles in the establishment and maintenance of a uniform lens fiber structure and in fiber organisation.

Here, I describe *kfrs4*, a spontaneous *Mip* mutation discovered in a strain derived from Kyoto Fancy Rat Stock No. 4 (KFRS4) [Kuramoto et al. 2010]. The *kfrs4* rats show bilateral congenital cataract with progressive severe degeneration of the lens fiber cells, similar to existing mouse *Mip* mutants; however, the cataract phenotype is inherited in a recessive fashion, unlike known *Mip* mutations in humans and mice. In this study, I performed

genetic, phenotypic and expression analyzes of the *kfrs4* mutant rats. My results suggest that this mutant should be classified as the first identified recessive mutant allele of *Mip*.

Materials and Methods

Ethics Statement

All of the procedures involving animals met the guidelines described in the Proper Conduct of Animal Experiments, as defined by the Science Council of Japan, and were approved by the Animal Care and Use Committee on the Ethics of the Tokyo Metropolitan Institute of Medical Science (Approval number: 14080 and 14081).

Rats

I used KFRS4/Kyo, BN/CrlCrlj, WIAR/lar and DOB/Oda rats as the wild-type rats in all of the experiments. KFRS4/Kyo and DOB/Oda rats were supplied by The National BioResource Project for the Rat in Japan (NBRP Rat: http://www.anim.med.kyoto-u.ac.jp/nbr/Default.aspx), Kyoto University (Kyoto, Japan). The BN/CrlCrlj and WIAR/Iar rats were purchased from Charles River Japan (Yokohama, Japan) and from the Institute for Animal Reproduction (Kasumigaura, Japan), respectively. All of the procedures involving animals met the guidelines described in the Proper Conduct of Animal Experiments, as defined by the Science Council of Japan, and were approved by the Animal Care and Use Committee of the Tokyo Metropolitan Institute of Medical Science, Tokyo University of Agriculture and Kyoto University.

Phenotypic analyses

The rat pupils were dilated using Mydrin-P (Santen Pharmaceutical, Osaka, Japan), and both eyes were observed after 5 min. The diagnosis of cataracts was performed by macroscopic examination, as described previously [Wada et al. 2011].

Both the right and left eyeballs from embryonic and postnatal wild-type, *kfrs4*/+ heterozygous and *kfrs4*/*kfrs4* homozygous rats were examined for histological analysis. The rats were sacrificed, and both eyeballs were enucleated and fixed in Superfix (Kurabo, Tokyo, Japan) overnight at room temperature (RT). After fixation, specimens were transferred to methanol, dehydrated, embedded in paraffin, and sectioned (5 μm). After removing the paraffin, the sections were stained with haematoxylin and eosin and observed under a Leica DM2500 light microscope.

Genetic mapping

Genetic mapping of the *kfrs4* mutant locus was performed by intercrossing progeny derived from the mating of (KFRS4/Kyo × DOB/Oda) F_1 × KFRS4/Kyo. The backcrossed progeny with a mutant phenotype were easily identified by the overt lens opacity induced by mydriatic instillation. DNA samples from 58 offspring, including 31 cataract-presenting rats of a KFRS4/Kyo and DOB/Oda cross, were genotyped using 108 polymorphic microsatellite markers selected from The NBRP Rat (Table 1) and six microsatellite markers (Table 2) developed from the rat genomic sequence (Ensembl:

http://asia.ensembl.org/Rattus_norvegicus/Info/Index). Genotyping was carried out using PCR (Table 3) and 4% agarose (3% Agarose XP and 1% Agarose S, Nippon gene, Tokyo, Japan) gel electrophoresis. The map position was refined using the Map Manager computer program [Manly et al. 2001].

Mutation analysis

A genomic fragment covering the four coding exons of *Mip* was amplified from genomic DNA isolated from wild-type rats (DOB/Oda, BN/CrlCrlj and WIAR/Iar), *kfrs4*/+ heterozygous rats (F_1 rats from a *kfrs4/kfrs4* and wild-type cross), and *kfrs4/kfrs4* homozygous rats. The primers Mip_F and Mip_R were used for amplification, and the following primers were used for sequencing: Mip_F1, Mip_F2, Mip_F3, Mip_F4, Mip_R1, and MIP_R2 (Table 3). The PCR products were purified using the QIAquick Gel Extraction Kit (Qiagen, Valencia, CA), sequenced using a BigDye Terminator kit (Life Technologies, Grand Island, NY) and analyzed using an Applied Biosystems 3130xl Genetic Analyzer.

The *kfrs4* allele was genotyped using PCR to amplify genomic DNA and fluorescently labeled using Mip_del_F and Mip_del_R (Table 3). DNA samples from 20 inbred rat strains (ACI/NKyo, DON/Kyo, IS/Kyo, RCS/Kyo, SHR/Kyo, TM/Kyo, W/Kyo, WAG/Kyo, WTC/Kyo, ZI/Kyo, KDP/Tky, LE/Stm, F344/Stm, DOB/Oda, KFRS2/Kyo, KFRS3A/Kyo, KFRS3B/Kyo, KFRS4/Kyo, KFRS5A/Kyo, and KFRS6/Kyo) for control of genotyping were supplied by NBRP Rat. The PCR products were separated using a Beckman

CEQ8000 instrument (Beckman Coulter, Fullerton, CA) with a size standard, and the fragment sizes were determined using fragment analysis software.

RT-PCR analysis of rats

Total RNA was isolated from the eyes of 7-week-old wild-type and *kfrs4*/*kfrs4* rats using TRIzol (Life Technologies) and the TRIzol Plus Purification Kit (Life Technologies) according to the manufacturers' protocols. The Superscript VILO cDNA synthesis kit (Life Technologies) was used to generate cDNA using 2 μg of DNase-pretreated total RNA. I also prepared cDNA from wild-type, *kfrs4*/+, and *kfrs4*/*kfrs4* rats at 7 and 10 weeks for quantitative RT-PCR (qRT-PCR). Primers for *Mip* (QT00387828) and *Gapdh* (QT00199633) were purchased from Qiagen (Valencia, CA). A total of 9 specific transcripts (*Cryaa*, *Crygb*, *Crygd*, *Casp6*, *Lim2*, *Bfsp1*, *Bfsp2*, *Gja3*, and *Gja8*) for lens fiber cells were used as the initial controls and to verify the quality of the fiber cells (Table 3). Subsequently, qRT-PCR was performed as previously described [Wada et al. 2011].

Antibodies

An anti-MIP rabbit polyclonal antibody (MIP-Cter) that targets a 17-amino acid (aa) peptide in the C-terminal cytoplasmic domain of MIP was previously characterized [Okamura et al. 2003; Golestaneh et al. 2004] and commercially acquired from Alpha Diagnostic International (San Antonio, TX). I also generated an anti-MIP rabbit polyclonal antibody

(MIP-Nter) to a peptide (C+TPPAVRGNLALNT) in the N-terminal region of the MIP peptide from aa 108 to 120 (NM_001105719). I used N-cadherin (CDH2) and β-catenin (CTNNB1) as markers of the lens. Both proteins were evenly expressed in lens fiber cells [Xu et al. 2002; Cain et al. 2008; Cooper et al. 2008; Cheng and Gong. 2011]. Mouse monoclonal anti-N-cadherin (CDH2) and anti-β-catenin (CTNNB1) antibodies were purchased from BD Biosciences (San Jose, CA). For a secondary antibody, Horseradish peroxidase (HRP)-conjugated donkey anti-rabbit and HRP-sheep anti-mouse IgG antibodies (GE Healthcare Life Science, Piscataway, NJ) were used for Western blotting. Alexa Fluor-conjugated secondary antibodies were obtained from Invitrogen (Life Technologies) .

Immunoblotting

Membrane proteins from the eyes of wild-type, *kfrs4*/+, and *kfrs4*/*kfrs4* rats at 7 and 8 weeks of age were purified as described by Sidjanin et al. [Sidjanin et al. 2001]. Samples containing approximately 500 ng of protein were separated on 15% SDS-polyacrylamide gels, and the separated proteins were transferred onto a Hybond-P PVDF membrane (GE Healthcare Life Science). MIP protein bands were detected using the anti-MIP-Cter (1:1,000) and -Nter (1:5,000) antibodies, followed by HRP-anti-rabbit (1:20,000) IgG secondary antibodies. ECL Prime Western blotting detection regents (GE Healthcare Life Science) were used for the enhanced chemiluminescent detection of specifically bound antibody, and the membrane was exposed to autoradiography film (GE Healthcare Life Science). The

membrane was then stripped and blotted with anti-CDH2 (1:2,000) and CTNNB1 (1:500) antibodies, followed by HRP-anti-mouse IgG secondary antibody (1:20,000) as a protein loading control. For quantitative Western blot analyses, the chemiluminescently labeled bands were quantified using the ImageJ software (http://rsb.info.nih.gov/ij). The expression level in wild-type rats was assigned an arbitrary value of 1, and the differences were evaluated using one-way ANOVA with a post hoc Bonferroni multiple comparison test.

Immunohistochemistry of the lens in rats

Both the right and left eyes from wild-type (9, 11 and 14 weeks of age), *kfrs4*/+ (8, 9, 11, 13 and 15 weeks of age), and *kfrs4/kfrs4* (9 and 11 weeks of age) rats were used for immunostaining. The procedure for immunohistochemistry of lens paraffin sections was described previously [Wada et al. 2011], and the sections were stained with anti-MIP-Cter (1:100), anti-MIP-Nter (1:100), anti-CDH2 (1:2,000) and anti-CTNNB1 (1:500). Fluorescence images were obtained using a Zeiss LSM780 confocal microscope and processed using Adobe Photoshop software. For each immunofluorescence labelling and lens fiber cell quantification experiment, I used three images from three different section preparations. The fluorescence intensity of MIP was analysed using the Image J software to analyze confocal images that were taken under identical conditions and adjusted using the intensity of CDH2 and CTNNB1 as a control. The expression level in wild-type rats was assigned an arbitrary value of 1, and differences were evaluated using a two-tailed *t*-test.

Results

Isolation and phenotypic characterisation of the spontaneous *kfrs4* mutant

While characterizing rats from the KFRS4/Kyo strain, I observed that all of the rats developed severe bilateral lens opacity throughout the eye within 7 weeks of birth (Figure 1A). To classify the cataract type caused by the *kfrs4* mutation, lenses from wild-type and KFRS4/Kyo rats were dissected and observed under dark-field microscopy (Figure 1B-E). The opacity of the KFRS4/Kyo rat lenses was observed in the anterior nuclear regions at P0 (Figure 1C). The cataract progressed to a nuclear cataract and then to an all-over opacity that included the cortical fibers at 7 weeks of age (Figure 1D). The F_1 progeny from the crossbreeding of DOB/Oda, BN/CrlCrlj, and WIAR/lar rats with KFRS4/Kyo rats showed normal lens phenotypes (Table 1). Crossbreeding between the (KFRS4/Kyo x DOB/Oda) F_1 rats and KFRS4/Kyo rats produced 31 offspring with cataract and 27 offspring without cataract. Moreover, mating (KFRS4/Kyo x WIAR/lar) F_1 rats with *kfrs4* rats produced 23 offspring with cataract and 29 offspring without cataract. These results indicate that the *kfrs4* mutation is recessive (Figure 1E, Table 1).

To define the histological defects in the lenses of *kfrs4* mutants, sagittal sections of the eye were prepared from wild-type, *kfrs4*/+, and *kfrs4/kfrs4* rats at various embryonic and postnatal stages (Figure 2). At E15.5, the phenotypes of the lens in *kfrs4/kfrs4* homozygotes showed a pattern of development similar to that of *kfrs4*/+ heterozygotes (Figure 2A, B).

However, there were signs of disorganisation in the fiber cells in the nuclear region of the *kfrs4/kfrs4* homozygous lens; the nuclei of the fiber cells remained in this region to a significant degree in comparison to the *kfrs4*/+ heterozygotes (Figure 2C, D). Degeneration of the lens fiber was pronounced in both the anterior and posterior regions in the *kfrs4/kfrs4* homozygotes at P0, with lens fiber swelling (Figure 2E, F). Over the next few weeks, the fiber cells became progressively more disorganized (Figure 2G, H), and irregularly shaped cells and huge vacuoles were present by 9 weeks of age (Figure 2I). In contrast, the lenses of *kfrs4*/+ heterozygotes exhibited compactly packed and uniform fiber cells at 19 weeks of age, similar to the lenses of wild-type rats (Figure 2J, K).

Identification of the *kfrs4* mutation

DNA samples from 58 [(KFRS4/Kyo × DOB/Oda) × KFRS4/Kyo] N_2 progeny (Table 1) were genotyped using 114 microsatellite markers (Table 2) on rat chromosome 1-20 to determine the location of the *kfrs4* mutation. Using this linkage analysis, I mapped the *kfrs4* mutation to an interval of approximately 9.7-Mb between markers *Cwf19l2* and *D7Wox43* on chromosome 7 (Figure 3A). This region contains more than 350 protein coding genes, including the *kfrs4* candidate region [Ensembl]. Given its genomic locus and its involvement in a similar mutant pathology in humans and mice, *Mip* was the strongest candidate gene for the *kfrs4* mutation. The *kfrs4* phenotype was non-recombinant with a microsatellite marker in the 3' region of *Mip* in 58 [(KFRS4/Kyo × DOB/Oda) ×KFRS4/Kyo]

N_2 progeny (Figure 3A).

By sequencing *Mip*, I identified a 5-bp insertion at nucleotide position 360 in exon 1 of *Mip* in the (KFRS4/Kyo × DOB/Oda) F_1 and KFRS4/Kyo rats (Figure 3B). This 5-bp insertion, AACAC, is present as a tandem repeat, most likely resulting from the duplication of the same 5 bp 5' of the insertion (Figure 3B). I designed a genotyping PCR primer pair to detect a 104-bp fragment for the wild-type *Mip* allele and a 109-bp fragment for the *kfrs4* allele. Based on these PCR amplicons, I was able to confirm the genotypes of the +/+, *kfrs4*/+, and *kfrs4/kfrs4* rats (Figure 3B). Moreover, the deletion was only observed in the *kfrs4* mutants and was not present among a set of 21 rat strains, including other KFRS strains (Figure 4).

The *kfrs4* 5-bp insertion is predicted to cause a frameshift mutation that results in truncation of the peptide chain by generating a stop codon at amino acid position 127, and this *kfrs4* frameshift mutation causes a truncation of the MIP protein that removes three transmembrane domains (*H4*, *H5* and *H6*), the *HE* hemichannels, cytoplasmic loop D, and extracellular loop E (Figure 5, 6A, B). To confirm this truncation of the C-terminal domain in *kfrs4* rats, I performed immunoblot and immunohistochemistry analyses using a rabbit polyclonal antibody, anti-MIP-Cter that targets a 17-amino acid (aa) peptide in the C-terminal cytoplasmic domain of MIP [Alpha Diagnostic International]. The 28-kDa (previously reported as the MIP band [Varadaraj et al. 2007]) bands were abundant in extracts from the wild-type and *kfrs4*/+ heterozygote eyes but were not detectable in the eye extracts from *kfrs4*

homozygotes (Figure 6C). Moreover, I generated an antibody, anti-MIP-Nter, to a peptide within an LC extracellular domain in the N-terminal region of the *kfrs4* mutation to detect the presence of the mutant MIP protein in *kfrs4* mutants. In the eye extracts of wild-type and *kfrs4*/+ rats, this antibody, as well as anti-MIP-Cter antibody, detected the 28-kDa band (Figure 6C). In addition, I detected a variant of approximately 23 kDa, which is suggested as partially degraded MIP by previous study [Swamy-Mruthinti 2001]. Although I have not yet identified whether these bands represent nonspecific antibody binding or a degradation product, these bands could not be detected in the eye extracts of *kfrs4*/*kfrs4* homozygotes.

As reported previously [Varadaraj et al. 2007], MIP was expressed throughout the fiber cells of the lens in wild-type rats; I also observed strong signals in the anterior fiber cells of adult rats (Figure 6D). The MIP staining was abolished in the *kfrs4* homozygous rats, confirming the truncation of the C-terminal domain in rats with the *kfrs4* mutation (Figure 6D). Immunohistochemistry using the anti-MIP-Nter antibody revealed a nearly identical staining pattern to that of anti-MIP-Cter (Figure 6E). I found that the staining of MIP is completely ablated in the *kfrs4*/*kfrs4* homozygotes.

Reduction in *Mip* mRNA and MIP protein expression by the *kfrs4* mutation

As mentioned above, the frameshift in the *kfrs4* mutant produces a truncated MIP protein that is missing several domains in the C-terminal region (Figure 5, 6). To examine the effect of the *kfrs4* mutation on *Mip* mRNA expression, I carried out real-time qRT-PCR using

RNA from wild-type, *kfrs4*/+ heterozygous, and *kfrs4/kfrs4* homozygous rats. The relative abundance of *Mip* transcripts in the eyes of *kfrs4*/+ and *kfrs4/kfrs4* rats was approximately 34.6 and 7.1 % of wild-type levels, respectively (Figure 7). To confirm this reduction of *Mip* mRNA in *kfrs4*/+ and *kfrs4/kfrs4* eyes and determine whether it caused a loss of lens fiber cells to induce cataracts, I performed qRT-PCR analysis of nine other lens-specific transcripts. Five of these transcripts, *Casp6, Lim2, Bfsp1,* and *Gja8,* did not exhibit significant expression changes among the wild-type, *kfrs4*/+, and *kfrs4/kfrs4* rats (Figure 7). The expression of three crystallins, *Cryaa*, *Crygd*, and *Crygd*, exhibited similar levels between the wild-type rats and the *kfrs4*/+ heterozygous rats, but significant reductions were detected in the *kfrs4/kfrs4* homozygous rats, suggesting the possibility that the reduction of these crystallins caused structural defects in the lens fiber cells of *kfrs4/kfrs4* homozygous rats. Although the expression of *Bfsp2* (a code lens structural protein) was lower in *kfrs4*/+ rats relative to wild-type, a change in expression was not detected in the *kfrs4/kfrs4* rats (Figure 7). These results suggest that the reduction of *Mip* expression in *kfrs4*/+ and *kfrs4/kfrs4* rats is not the result of cataract formation but is instead caused by the reduced expression of certain genes that were affected in the *kfrs4* mutant. *Gja3* (also known as connexin 46) showed a significantly lower expression in *kfrs4*/+ and *kfrs4/kfrs4* rats compared with wild-type (Figure 7). Although I could not explain why the expression of *Gja3* is also reduced in *kfrs4*/+ heterozygous and *kfrs4/kfrs4* homozygous rats, the GJA3 protein directly interacts with MIP, mediated by the C-terminal region [Yu et al. 2005]; therefore, it may be an effect of the

reduction in *Mip* mRNA as a result of the *kfrs4* mutation.

Quantitative immunoblotting and immunohistochemistry were also performed to confirm the MIP protein expression levels in wild-type and *kfrs4*/+ heterozygous rats. Although the difference in protein levels was not significant according to a statistical analysis, MIP was 1.59 times less abundant in *kfrs4*/+ eyes than in wild-type eyes (Figure 8). Quantitative immunohistochemical analysis of MIP in the fiber cells of the anterior lens revealed that the expression level of MIP significantly decreased in the *kfrs4*/+ rat, whereas the level of CDH2 did not decrease (Figure 9A). As shown in Figure 9B, the amount of MIP in *kfrs4*/+ eyes was 33.1% of the level observed in wild-type eyes. Similar results were obtained using the anti-MIP-Nter antibody and CTNNB1 as control for quantitative analysis (Figure 8, 9C-H).

Discussion

I presented several lines of evidence demonstrating that a mutation in the *Mip* gene underlies congenital cataract in *kfrs4* mutant rats. First, *Mip* is located within the candidate region identified for the *kfrs4* mutation (Figure 3A). Second, the *kfrs4* mutant phenotypes were consistent with the *Mip* mutation genotypes in all of the rats examined (Figure 3B, Figure 4). Third, the absence of MIP-positive bands in the Western blots and MIP-specific immunofluorescence in eye sections from *kfrs4* mutants indicate the absence of the normal *Mip* gene product (Figure 6B-G). The identified mutation is a 5-bp nucleotide insertion within the coding region of the amino terminus of MIP, adding to the catalog of known *Mip* mutations that cause cataract in mammals.

In human and mice, point mutations [Shiels and Bassnett. 1996; Berry et al. 2000; Gu et al. 2007; Lin et al. 2007; Wang et al. 2010; Wang et al. 2011; Yang et al. 2011], intragenic in-frame deletions [Sidjanin et al. 2001; Okamura et al. 2003] and frameshift mutations [Shiels and Bassnett. 1996; Geyer et al. 2006] in *Mip* have been characterized to cause dominant phenotypes (Figure 5). The cataract phenotype in $Mip^{Hfi/+}$ heterozygous mice suggested that a 76-bp deletion in *Mip* is a gain-of-function mutation, consistent with data showing that a normal level of wild-type MIP protein expression observed in $Mip^{Hfi/+}$ could not protect the lens from cataract formation [Sidjanin et al. 2001]. Another *Mip* mutation in mice, $Mip^{Cat\text{-}Tohm}$ is a 12-bp deletion in *Mip* that does not alter the open reading frame, but

these mutant mice exhibited a more severe cataract phenotype than did *Mip* knockout mice [Shiels et al. 2001; Al-Ghoul et al. 2003] with a null mutation in *Mip* [Bermejo and, Martínez-Frías. 1998]. Interestingly, the lens fiber cells of a transgenic mouse that expressed both the wild-type and the $Mip^{Cat\text{-}Tohm}$ mutated *Mip* showed more severe degeneration at birth than did the lens cells of $Mip^{Cat\text{-}Tohm/Cat\text{-}Tohm}$ homozygotes, which expressed only $Mip^{Cat\text{-}Tohm}$. In addition, the E134G/T138R mutant of human *MIP* leads to congenital cataract and results in a loss of water permeability owing to a failure in protein trafficking to the plasma membrane in homozygotes [Berry et al. 2000]; however, when the E134G/T138R mutant is co-expressed with wild-type MIP protein, the mutant protein reaches the plasma membrane but causes tetramer instability and a loss-of-function of wild-type MIP [Francis et al. 2000]. Moreover, FRET analysis of human Mip^{ADC2} and wild-type MIP coexpressed in mammalian cells demonstrated that this mutation is dominant because the hetero-oligomerization of the wild-type and mutant MIP molecules traps the wild-type MIP in the endoplasmic reticulum [Varadaraj et al. 2008]. These studies indicate that mutated versions of the MIP protein have a strong dominant-negative effect on lens transparency and that cataract in these mouse and human cases is caused by neomorph mutations. However, I characterized *kfrs4* as a recessive mutation because *kfrs4*/+ heterozygous rats exhibit a lens structure that is similar to that of wild-type rats until the late stages of development (Figure 1, 2, Table 1), and the *kfrs4* mutation was effectively mapped in a linkage study using backcrosses to follow the recessive phenotype (Figure 3A). The *kfrs4*/+ heterozygous and *kfrs4/kfrs4* homozygous rats appear to

have reduced *Mip* mRNA expression (Figure 7). Moreover, the mutant MIP protein in *kfrs4* rats presumably lacks 136 aa from the C-terminus because MIP signals were not detected by Western blotting and immunohistochemistry when an anti-MIP-Cter antibody that recognise C-terminal region of MIP was used (Figure 6, 8). These results suggest that the frameshift caused by the *kfrs4* mutation leads to though the rapid degradation of mRNA by NMD; this observation supports the characterisation of *kfrs4* as a loss-of-function mutation in *Mip*.

Acknowledgments

The author would like to express my sincere gratitude to my supervisor, Professor Jun-ichi Hayashi for providing me this precious study opportunity as a Ph.D student in his laboratory. The author particularly appreciates Dr. Yoshiaki Kikkawa, Tokyo Metropolitan Institute of Medical Science for stimulating discussion and technical advices throughout this study. The author greatly appreciates Dr. Kenta Wada, Tokyo University of Agriculture for providing invaluable data and informative advices. The author also appreciates Dr. Hiroshi Shitara for production of the *Mip* mutant mice. The author also appreciates Dr. Choji Taya and other staffs of animal facility, Tokyo Metropolitan Institute of Medical Science for maintaining of rats and mice; Dr. Tadao Serikawa and Dr. Takashi Kuramoto, Kyoto University for providing the KFRS4/Kyo rats and DNA samples of 20 inbred rats; Dr. Sen-ichi Oda, Okayama University of Science for providing the DOB/Oda strain; and Ms. Tomoko Ohashi, Ms. Saki Okubo, Mr. Kensuke Takekuma and Dr. Ryoichi Hashizume, Tokyo University of Agriculture for they skilled technical assistance in this work. Finally, I thank members of Mammalian Genetics Project of Tokyo Metropolitan Institute of Medical Science for valuable suggestions and supporting in this work.

References

1 Al-Ghoul KJ, Kirk T, Kuszak AJ, Zoltoski RK, Shiels A, Kuszak JR. (2003) Lens structure in MIP-deficient mice. Anat Rec A Discov Mol Cell Evol Biol 273: 714-730.

2 Bermejo E, Martínez-Frías ML. (1998) Congenital eye malformations: clinical-epidemiological analysis of 1,124,654 consecutive births in Spain. Am J Med Genet 17: 497-504.

3 Berry V, Francis P, Kaushal S, Moore A, Bhattacharya S (2000) Missense mutations in MIP underlie autosomal dominant 'polymorphic' and lamellar cataracts linked to 12q. Nat Genet. 25: 15-17.

4 Bloemendal H, Zweers A, Vermorken F, Dunia I, Benedetti EL (1972) The plasma membranes of eye lens fibres. Biochemical and structural characterization. Cell Differ 91-106.

5 Cain S, Martinez G, Kokkinos MI, Turner K, Richardson RJ, Abud HE, Huelsken J, Robinson ML, de Iongh RU. (2008) Differential requirement for beta-catenin in epithelial and fiber cells during lens development. Dev Biol 321: 420–433.

6 Cheng C, Gong X (2011) Diverse roles of Eph/ephrin signaling in the mouse lens. PLoS One 6: e28147.

7 Chepelinsky AB (2009) Structural function of MIP/aquaporin 0 in the eye lens; genetic defects lead to congenital inherited cataracts. Handb Exp Pharmacol. 190: 265-297.

8 Cooper MA, Son AI, Komlos D, Sun Y, Kleiman NJ, Zhou R. (2008) Loss of ephrin-A5 function disrupts lens fiber cell packing and leads to cataract. Proc Natl Acad Sci U S A 105: 16620–16625.

9 Ding X, Zhou N, Lin H, Chen J, Zhao C, Zhou G, Hejtmancik JF, Qi Y (2014) A novel MIP gene mutation analysis in a Chinese family affected with congenital progressive punctate cataract. PLoS One 9: e102733.

10 Francis P, Chung JJ, Yasui M, Berry V, Moore A, Wyatt MK, Wistow G, Bhattacharya SS, Agre P. (2000) Functional impairment of lens aquaporin in two families with dominantly inherited cataracts. Hum Mol Genet 9: 2329-2334.

11 Geyer DD, Spence MA, Johannes M, Flodman P, Clancy KP, Berry R, Sparkes RS, Jonsen MD, Isenberg SJ, Bateman JB (2006) Novel single-base deletional mutation in major intrinsic protein (MIP) in autosomal dominant cataract. Am J Ophthalmol 141: 761-763.

12 Golestaneh N, Fan J, Fariss RN, Lo WK, Zelenka PS, Chepelinsky AB. (2004) Lens major intrinsic protein (MIP)/aquaporin 0 expression in rat lens epithelia explants requires fibroblast growth factor-induced ERK and JNK signaling. J Biol Chem 279: 31813-31822.

13 Gorin MB, Yancey SB, Cline J, Revel JP, Horwitz J (1984) The major intrinsic protein (MIP) of the bovine lens fiber membrane: characterization and structure based on cDNA cloning. Cell 39: 49-59.

14 Gu F, Zhai H, Li D, Zhao L, Li C, Huang S, Ma X (2007) A novel mutation in major intrinsic protein of the lens gene (MIP) underlies autosomal dominant cataract in a Chinese

family. Mol Vis 13: 1651-1656.

15 Hejtmancik JF, Smaoui N. (2003) Molecular genetics of cataract. Dev Ophthalmol.; 37:67-82.

16 Kumari SS, Varadaraj K (2009) Intact AQP0 performs cell-to-cell adhesion. Biochem Biophys Res Commun 390: 1034-1039.

17 Kuramoto T, Yokoe M, Yagasaki K, Kawaguchi T, Kumafuji K, Serikawa T. (2010) Genetic analyses of fancy rat-derived mutations. Exp Anim 59: 147-155.

18 Lin H, Hejtmancik JF, Qi Y (2007) A substitution of arginine to lysine at the COOH-terminus of MIP caused a different binocular phenotype in a congenital cataract family. Mol Vis 13: 1822-1827.

19 Mali P, Yang L, Esvelt KM, Aach J, Guell M, DiCarlo JE, Norville JE, Church GM. (2013) RNA-guided human genome engineering via Cas9. Science 339: 823-826.

20 Manly KF, Cudmore RH Jr, Meer JM (2001) Map Manager QTX, cross-platform software for genetic mapping. Mamm Genome 12: 930-932.

21 Okamura T, Miyoshi I, Takahashi K, Mototani Y, Ishigaki S, Kon Y, Kasai N. (2003) Bilateral congenital cataracts result from a gain-of-function mutation in the gene for aquaporin-0 in mice. Genomics 81: 361-368.

22 Santana A, Waiswo M (2011) The genetic and molecular basis of congenital cataract. Arq Bras Oftalmol 74: 136-142.

23 Shiels A, Bassnett S (1996) Mutations in the founder of the MIP gene family underlie

cataract development in the mouse. Nat Genet 12: 212-215.

24 Shiels A, Bassnett S, Varadaraj K, Mathias R, Al-Ghoul K, et al. (2001) Optical dysfunction of the crystalline lens in aquaporin-0-deficient mice. Physiol Genomics 7: 179-186.

25 Sidjanin DJ, Parker-Wilson DM, Neuhäuser-Klaus A, Pretsch W, Favor J, Deen PM, Ohtaka-Maruyama C, Lu Y, Bragin A, Skach WR, Chepelinsky AB, Grimes PA, Stambolian DE. (2001) A 76-bp deletion in the Mip gene causes autosomal dominant cataract in Hfi mice. Genomics 74: 313-319.

26 Swamy-Mruthinti S (2001) Glycation decreases calmodulin binding to lens transmembrane protein, MIP. Biochim Biophys Acta. 2001 Apr 1536: 64-72.

27 Varadaraj K, Kumari SS, Mathias RT. (2007) Functional expression of aquaporins in embryonic, postnatal, and adult mouse lenses. Dev Dyn 236: 1319-1328.

28 Varadaraj K, Kumari SS, Mathias RT (2010) Transgenic expression of AQP1 in the fiber cells of AQP0 knockout mouse: effects on lens transparency. Exp Eye Res 91: 393-404.

29 Varadaraj K, Kumari SS, Patil R, Wax MB, Mathias RT. (2008) Functional characterization of a human aquaporin 0 mutation that leads to a congenital dominant lens cataract. Exp Eye Res 87: 9-21.

30 Wada K, Maeda YY, Watanabe K, Oshio T, Ueda T Takahashi G, Yokohama M, Saito J, Seki Y, Takahama S, Ishii R, Shitara H, Taya C, Yonekawa H, Kikkawa Y (2011) A deletion in a cis element of Foxe3 causes cataracts and microphthalmia in rct mice. Mamm Genome

22: 693-702.

31 Wang H, Yang H, Shivalila CS, Dawlaty MM, Cheng AW, Zhang F, Jaenisch R. (2013) One-step generation of mice carrying mutations in multiple genes by CRISPR/Cas-mediated genome engineering. Cell 153: 910-918.

32 Wang KJ, Li SS, Yun B, Ma WX, Jiang TG, Zhu SQ (2011) A novel mutation in MIP associated with congenital nuclear cataract in a Chinese family. Mol Vis 17: 70-77.

33 Wang W, Jiang J, Zhu Y, Li J, Jin C, Shentu X, Yao K (2010) A novel mutation in the major intrinsic protein (MIP) associated with autosomal dominant congenital cataracts in a Chinese family. Mol Vis 16: 534-539.

34 Xu L, Overbeek PA, Reneker LW (2002) Systematic analysis of E-, N- and Pcadherin expression in mouse eye development. Exp Eye Res 74: 753–760.

35 Yang G, Zhang G, Wu Q, Zhao J (2011) A novel mutation in the MIP gene is associated with autosomal dominant congenital nuclear cataract in a Chinese family. Mol Vis 17: 1320-1323.

36 Yoshimi K, Kaneko T, Voigt B, Mashimo T. (2014) Allele-specific genome editing and correction of disease-associated phenotypes in rats using the CRISPR-Cas platform. Nat Commun 5: 4240.

37 Yu XS, Yin X, Lafer EM, Jiang JX (2005) Developmental regulation of the direct interaction between the intracellular loop of connexin 45.6 and the C terminus of major intrinsic protein (aquaporin-0). J Biol Chem 280: 22081-22090.

38 Yu Y, Yu Y, Chen P, Li J, Zhu Y, Zhai Y, Yao K (2014) A novel MIP gene mutation associated with autosomal dominant congenital cataracts in a Chinese family. BMC Med Genet 15: 6.

Figure 1. Lens opacities in *kfrs4* mutant rats. A. Gross appearance in *kfrs4* rats at 7 weeks of age. Opacity was observed throughout the eye (right). **B-E.** Dark field imaging of the dissected lens from DOB/Oda (+/+, **B**), KFRS4/Kyo (*kfrs4/kfrs4*, **C, D**), and (KFRS4/Kyo x DOB/Oda) F_1 (*kfrs4*/+, **E**) rats. Wild-type rats show normal transparency (**B**), but nuclear opacity is observed in the anterior (left) and side (right) views in a lens from a *kfrs4/kfrs4* homozygote at P0 (**C**). The *kfrs4/kfrs4* homozygous rat developed a dense nuclear cataract with full penetrance at 7 weeks of age (**D**). At 17 weeks of age, both *kfrs4*/+ heterozygotes and +/+ rats showed normal lens transparency (**E**). (Watanabe et al. 2012 PLoS One)

Figure 2. Lens phenotypes in +/+, *kfrs4*/+, and *kfrs4/kfrs4* rats at various embryonic and postnatal stages. Eyes were fixed, sectioned, and stained with haematoxylin and eosin. **A-D.** Lens histology in *kfrs4*/+ (**A, C**) and *kfrs4/kfrs4* (**B, D**) rats at E15.5. Highly magnified images of the dotted box area in **A** and **B** of the lens fibers in *kfrs4*/+ (**C**) and *kfrs4/kfrs4* (**D**) rats are shown. C, cornea; N, nuclear region. **E-K.** Lens histology in +/+, *kfrs4*/+ and *kfrs4/kfrs4* rats at various postnatal stages. **E-F.** Comparison of phenotypes of the anterior fibers between +/+ (**E**) and *kfrs4/kfrs4* (**F**) rats at P0. LFC, lens fiber cell. **G-K.** Mature lens fibers in +/+ (**J**), *kfrs4*/+ (**G, K**) and *kfrs4/kfrs4* (**H, I**) rats. Large vacuoles (asterisk) were observed in the lens fibers of *kfrs4/kfrs4* rats at 9 weeks of age (**I**). ALE, anterior lens epithelium. Scale bar = 200 μm. (Watanabe et al. 2012 PLoS One)

Figure 3. Positional cloning of the *kfrs4* mutation. A. Haplotype analysis for (KFRS4/Kyo × DOB/Oda) F_1 × KFRS4/Kyo backcross progeny in the proximal region of chromosome 7. Markers are shown to the left. The number of offspring inheriting each type of chromosome is listed at the bottom of each column. **B.** Mutation analysis of *Mip* in the KFRS4/Kyo rat. Sequence analysis (left panels) for exon 1 of *Mip* in DOB/Oda (+/+, top), (KFRS4/Kyo x DOB/Oda) F_1 (*kfrs4*/+, middle), KFRS4/Kyo (*kfrs4/kfrs4*, bottom) rats. A 5-bp insertion (AACAC, pink and dark orange labeled in the bottom panel) is found in *kfrs4*/+ and *kfrs4*/*kfrs4* rats. A size analysis (right panels) of fragments across the deletion revealed a 109-bp amplicon in the homozygous *kfrs4/kfrs4* rats (bottom) compared with a 104-bp amplicon in the +/+ rats (top); both amplicons were present in the *kfrs4*/+ rats (middle). (Watanabe et al. 2012 PLoS One)

Figure 4. Gain of the 5-bp insertion in exon 1 of *Mip* in a KFRS4/Kyo strain. Genotyping of various wild-type strains of rat, including other KFRS strains (asterisks), revealed an absence of the 5-bp insertion. (Watanabe et al. 2012 PLoS One)

Figure 5. Alignment of MIP amino acid sequences and mutations in *Mip* responsible for congenital cataract in humans, mice and rats. Amino acid sequences of human MIP (GenBank accession no. NM_012064) identical to those of mouse (NM_008600) and rat MIP (NM_001105719) are shown as dots. The numbers at the top of the human sequence indicate

nucleotide positions. The locations of the six transmembrane domains (*H1, H2, H3, H4, H5,* and *H6*) and two hemichannels (*HB* and *HE*) are indicated by underlines and dotted underlines, respectively. The locations of the extracellular loops (Loop A, C, and E) and intracellular loops (Loop B and D) are indicated between the corresponding transmembrane domains. Eight reported human mutations, four reported mouse mutations, and the *kfrs4* rat mutation are indicated in green, blue, and red, respectively. (Watanabe et al. 2012 PLoS One)

Figure 6. The *kfrs4* mutation produces a frameshift and the generation of a C-terminally truncated MIP protein. A, B. Predicted structures of the MIP proteins encoded by the wild-type (**A**) and *kfrs4* mutant (**B**) alleles. A schematic diagram showing the presumed membrane topology of MIP (modified from Francis et al. [Francis et al. 2000]). The locations of the six transmembrane domains (*H1, H2, H3, H4, H5,* and *H6*), two hemichannels (*HB* and *HE*), and the extracellular (*LA, LC,* and *LE*) and intracellular (*LB* and *LD*) loops are indicated. The schematic illustrates premature truncation of the protein expressed from the Mip^{kfrs4} allele as a result of the mutation (**B**). **C.** Western blots of homogenates prepared from the eyes of +/+, *kfrs4*/+ and *kfrs4/kfrs4* mutant rats detected with anti-MIP-Cter (top) and anti-MIP-Nter (middle) antibodies. Note the absence of a specific band at ~28 kDa (arrows) in the *kfrs4/kfrs4* mutant homogenates. The samples were processed for indirect immunofluorescence using an anti-CNTTB1 antibody (bottom). **D, E.** Immunofluorescence labelling of MIP in the lens of +/+ (left panels) and *kfrs4/kfrs4* (right panels) rats at 7 weeks of

age. These panels show merged images of the detection of MIP (red) + CNTTB1 (green) + DAPI (blue). The small panels within the large panels show higher magnifications of the dashed boxed areas in the large panels. ALE, anterior lens epithelium. Scale bars = 200 μm (large panels) and 50 μm (small panels). (Watanabe et al. 2012 PLoS One)

Figure 7. Quantitative analysis of *Mip* and selected lens fiber specific gene expression in lenses from +/+, *kfrs4*/+, and *kfrs4/kfrs4* rats. A. Relative levels of mRNA in the lenses of +/+ (blue bars), *kfrs4*/+ (orange bars), and *kfrs4/kfrs4* (red bars) rats at 7 weeks of age. mRNA expression was detected using real-time quantitative RT-PCR analysis. (n = 3) *P < 0.05, **P < 0.01, ***P < 0.001. (Watanabe et al. 2012 PLoS One)

Figure 8. Quantitative analysis of MIP protein expression in lenses from +/+ and *kfrs4*/+ rats by Western blot analyses. Densitometric quantification of MIP expression levels detected by Western blot analysis using the anti-MIP-Cter and anti-MIP-Nter antibodies in the eyes of +/+ and *kfrs4*/+ rats at 7 weeks of age. Protein integrity was confirmed with the CDH2 and CNTTB1 as a control (Modified from Watanabe et al. 2012 PLoS One).

Figure 9. Quantitative analysis of MIP protein expression in lenses from +/+ and *kfrs4*/+ rats by immunohistochemical analyses. A, C. Immunofluorescence labelling of CDH2 (top), MIP (middle), and merged images (bottom) in the lens fibers from +/+ (left) and *kfrs4*/+

(right) rats at 8 weeks of age. The sections are stained by both anti-MIP-Cter (**A**) and anti-MIP-Nter (**C**) antibodies. Scale bar = 20 μm. **B, D.** Quantification of MIP intensities in **A** and **C**. **E, G.** Immunofluorescence labelling of CNTTB1 (top), MIP (middle), and merged images (bottom) in the lens fibers from +/+ (left) and *kfrs4*/+ (right) rats at 8 weeks of age. The sections are stained by both anti-MIP-Cter (**E**) and anti-MIP-Nter (**G**) antibodies. Scale bar = 20 μm. **F, H.** Quantification of MIP intensities in **E** and **G**. The values shown in each graph indicate the mean relative expression levels and the standard errors of triplicate samples (n = 3). **P < 0.01, ***P < 0.001, n.s., not significant. (Modified from Watanabe et al. 2012 PLoS One)

Figure 10. Genome-editing of *Mip* in mice. A. Schematic representation of the Cas9/gRNA-targeting site in *Mip*. The sg-RNA-targeting sequence and PAM sequence are labeled in red and blue, respectively. The *Pvu*II restriction site at the target region is underlined. Arrows indicate mutation sites of the human and rat, respectively. **B.** Genotyping of 22 offspring produced by Cas9-mediated cleavage at *Mip* in mice. The top and bottom panels show the SSLP and RFLP patterns, respectively. M, marker (100 bp ladder); N, negative control (DDW).

Figure 11. The sequences of mutated alleles from the offspring genome-edited by

CRISPR/Cas9. The sg-RNA targeting sequence and PAM sequence are highlighted in yellow and green, respectively, in sequence of B6J mice. The nucleotide codes of two- and three-mixed bases are labeled in red and blue, respectively.

Figure 12. Sequences of mutated alleles in *Mip* mutation sites of CRISPR/Cas9-mediated genome-edited mice. The sg-RNA-targeting sequence and PAM sequence are labeled in red and blue, respectively. The substitution, deletion (dashes), and insertion sites are labeled in green.

Figure 13. Predicted amino acid sequences of *Mip* mutant mice.

Figure 14. Establishment of the $Mip^{A111EfsX3}$ and $Mip^{Y105SfsX4}$ mice. A. PCR-RFLP patterns of the $Mip^{A111EfsX3/+}$ heterozygous, $Mip^{A111EfsX3/A111EfsX3}$ homozygous, $Mip^{Y105SfsX4/+}$ heterozygous, $Mip^{Y105SfsX4/Y105SfsX4}$ homozygous, and wild-type B6J mice. The *Pvu*II digestion of PCR products from wild-type mice produces bands at 151- and 83-bp. However, $Mip^{A111EfsX3/A111EfsX3}$ and $Mip^{Y105SfsX4/Y105SfsX4}$ mice are homozygous for the disruption of the *Pvu*II site and yield only a single 227- and 212-bp band, respectively, whereas the $Mip^{A111EfsX3/A110EfsX3}$ and $Mip^{Y105SfsX4/Y105SfsX4}$ mice are heterozygous for the mutation as shown by the two banding patterns superimposed on one another. M, marker (100 bp ladder). **B.** The sequences of mutated alleles from B6J (top), $Mip^{A111EfsX3/A111EfsX3}$ (middle), and

Mip$^{Y105SfsX4/Y105SfsX4}$ (bottom) homozygous mice. Asterisks indicate stop codon. **C.** Alignment of the predicted amino acid sequences in wild-type, *Mip*^{A111EfsX3} and *Mip*^{Y105SfsX4} mice, *MIP*$^{337C>T}$ human, and *Mip*$^{359\_360insAACAC}$ Rat (*kfrs4*).

Figure 15. Expression analyses of MIP protein in *Mip*$^{+/+}$, *Mip*$^{Y105SfsX4/+}$ heterozygous and *Mip*$^{Y105SfsX4/Y105SfsX4}$ homozygous mice at 12 weeks of age. Immunohistochemistry of the eye sections from *Mip*$^{+/+}$ (A), *Mip*$^{Y105SfsX4/+}$ (B) and *Mip*$^{Y105SfsX4/Y105SfsX4}$ (C) mice stained with CTNNB1 (green), anti-MIP-Cter (red) antibodies and DAPI (blue). The small panels within the large panels show higher magnifications of the anterior poles including the anterior lens epithelium (ALE). Scale bar = 50 μm.

Figure 16. Lens phenotypes in *Mip*^{Y105SfsX4} mice. A-C. Dark field imaging of the dissected lens from *Mip*$^{+/+}$ (**A**), *Mip*$^{Y105SfsX4/+}$ heterozygous (**B**) and *Mip*$^{Y105SfsX4/Y105SfsX4}$ homozygous (**C**) mice at 12 weeks of age. **D-I.** Histological analysis in the *Mip*$^{+/+}$ (**D, G**), *Mip*$^{Y105SfsX4/+}$ (**E, H**) and *Mip*$^{Y105SfsX4/Y105SfsX4}$ (**F, I**) mice at 12 weeks of age. The eye sections are stained by Hematoxylin-eosin. Highly magnified images of anterior poles of lens including the anterior lens epithelium (ALE) in **D-F** are shown in **G-I**. **J-M**. Lens fibers from the anterior poles (AP, **J-L**) and equator regions (ER, **M-O**) visualized by immunohistochemistry of CTNNB1 in the *Mip*$^{+/+}$ (**J, M**), *Mip*$^{Y105SfsX4/+}$ (**K, N**) and *Mip*$^{Y105SfsX4/Y105SfsX4}$ (**L, O**) mice. Scale bar = 1 mm (**A-C**), 100 μm (**D-I**) and 50 μm (**J-O**).

Figure 17. Expression analysis of *Mip* transcripts in *Mip*^{A111EfsX3} mice and *Mip*^{kfrs4} rats. A. Semiquantitative RT-PCR analysis of *Mip* expression in the eye of mice (*Mip*$^{+/+}$, *Mip*$^{A111EfsX3/+}$ heterozygote and *Mip*$^{A111EfsX3/A111EfsX3}$ homozygote) and rats (*Mip*$^{+/+}$, *Mip*$^{kfrs4/+}$ heterozygote and *Mip*$^{kfrs4/kfrs4}$ homozygote) at P0. The upper panel shows 92-bp RT-PCR products from *Mip*-specific primers (Mip_c240-259F and Mip_c308-332R) in both mice and rats. The integrity of the cDNA was confirmed using a *Gapdh* control band (bottom panel). **B.** Relative levels of *Mip* mRNA in the eye of mice (*Mip*$^{+/+}$, *Mip*$^{A111EfsX3/+}$ and *Mip*$^{A111EfsX3/A111EfsX3}$) and rats (*Mip*$^{+/+}$, *Mip*$^{kfrs4/+}$ and *Mip*$^{kfrs4/kfrs4}$) at P0. *Cdh23* mRNA expression was measured by real-time RT-PCR analysis using primers of the Mip_c636-656 and Mip_c721-743R (Table 3). The expression levels in both *Mip*$^{+/+}$ mice and rats were assigned an arbitrary value of 1 for comparative purposes. He, homozygotes; Ho, homozygotes. *$P < 0.05$; **$P < 0.01$.

Table 1. Incidence of cataractogenesis in *kfrs4* F_1 rats from crosses of KFRS4/Kyo and 3 inbred lines and in [(KFRS4/Kyo × DOB/Oda) F_1 × KFRS4/Kyo] N_2, and [(KFRS4/Kyo × WIAR/Iar) F_1 × KFRS4/Kyo] N_2 rats.

Cross	Weeks of age	n	Phenotype		Incidence (%)
			Cataract (n)	Normal (n)	
KFRS4/Kyo	8	55	55	0	100
(KFRS4/Kyo × DOB/Oda)F_1	12	33	0	33	0
	44	3	0	3	0
[(KFRS4/Kyo × DOB/Oda)F_1 × KFRS4]N_2	12	58	31	27	53.4
(KFRS4/Kyo × BN/CrlCrlj)F_1	14	2	0	2	0
(KFRS4/Kyo × WIAR/Iar)F_1	19	31	0	31	0
[(KFRS4/Kyo × WIAR/Iar)F_1 × KFRS4]N_2	12	52	23	29	44.2

Table 2. Microsatellite markers used in genetic mapping of the rat *kfrs4* locus.

Chr	Marker	Position		
1	*D1Rat5*	10818666	-	10818827
1	*D1Rat20*	48777690	-	48777853
1	*D1Rat410*	87625119	-	87625270
1	*D1Rat214*	100034565	-	100034664
1	*D1Rat320*	119536685	-	119536913
2	*D2Rat187*	178078	-	178209
2	*D2Rat253*	25663275	-	25663463
2	*D2Rat287*	199883673	-	199883885
2	*D2Rat222*	145318604	-	145318823
2	*D2Rat52*	200866668	-	200866813
2	*D2Rat88*	222281737	-	222281876
2	*D2Rat250*	249990265	-	249990446
3	*D3Rat56*	3577906	-	3578102
3	*D3Rat193*	10016017	-	10016173
3	*D3Rat169*	unknown		
3	*D3Rat34*	74394822	-	74394967
3	*D3Rat176*	81470283	-	81470426
3	*D3Arb10*	88944877	-	88945187
3	*D3Rat204*	101934371	-	101934633
3	*D3Mit2*	143214619	-	143214737
3	*D3Rat114*	149496486	-	149496698
4	*D4Rat17*	45810174	-	45810272
4	*D4Arb10*	61646623	-	61647018
4	*D4Rat48*	unknown		
4	*D4Mgh18*	128179958	-	128180046
4	*D4Arb15*	158101749	-	158101963
4	*D4Mgh13*	181442881	-	181443052
5	*D5Rat116*	1220774	-	1221009
5	*D5Rat128*	unknown		
5	*D5Rat147*	86116639	-	86116811
5	*D5Rat98*	100017061	-	100017265
5	*D5Rat71*	115431931	-	115432142
5	*D5Rat95*	130642376	-	130642474

Table 2. Continued.

Chr	Marker	Position		
5	*D5Rat36*	145186818	-	145187033
6	*D6Rat62*	5533081	-	5533298
6	*D6Rat149*	7161391	-	7161540
6	*D6Mit1*	98840517	-	98840644
6	*D6Rat12*	114032010	-	114032160
6	*D14Mgh4*	138229582	-	138229831
7	*D7Mgh11*	2026569	-	2026705
7	*D7Rat39*	4936704	-	4936848
7	*D7Wox43*	10129572		10129731
7	*D7Got4*	10169231	-	10169371
7	*D7Uwm1*	19259382	-	19259619
7	*D7Got17*	28488437	-	28488625
7	*D7Got31*	39557830	-	39557975
7	*D7Rat164*	69506937	-	69507070
7	*D7Got56*	79283387	-	79283565
7	*D7Rat184*	unknown		
7	*D7Rat42*	88994909	-	88995082
7	*D7Rat128*	121523978	-	121524220
7	*D7Rat81*	129500285	-	129500555
8	*D8Rat184*	64617024	-	64617185
8	*D8Rat184*	64617024	-	64617185
8	*D8Rat16*	98878558	-	98878727
8	*D8Rat8*	117988094	-	117988418
9	*D9Rat132*	11099462	-	11099609
9	*D9Rat158*	23881722	-	23881993
9	*D9Rat22*	52292953	-	52293093
9	*D9Mit3*	55475966	-	55476135
9	*D9Mit7*	87490923	-	87491097
10	*D10Rat198*	14824852	-	14825065
10	*D10Rat104*	41968132	-	41968305
10	*D10Rat93*	81887168	-	81887390
11	*D11Rat52*	6229317	-	6229477
11	*D11Rat21*	25035084	-	25035273

Table 2. Continued.

Chr	Marker	Position		
11	*D11Rat97*	35072773	-	35072900
11	*D11Rat63*	67659790	-	67659992
11	*D11Arb4*	68234775	-	68235010
11	*D11Rat92*	76129817	-	76129943
12	*D12Arb13*	7382722	-	7382953
12	*D12Rat15*	29369537	-	29369703
13	*D13Rat5*	8292944	-	8293105
13	*D13Rat1*	10555731	-	10556042
13	*D13Rat21*	43835058	-	43835207
14	*D14Rat1*	4895895	-	4896036
14	*D14Rat75*	12118228	-	12118490
14	*D14Rat78*	17564856	-	17564965
14	*D14Rat7*	24684071	-	24684244
14	*D14Rat45*	70233190	-	70233365
14	*D14Rat110*	107119264	-	107119581
15	*D15Rat17*	45042675	-	45042874
16	*D16Rat80*	14559475	-	14559634
16	*D16Mit5*	unknown		
16	*D16Rat85*	12513036	-	12513180
16	*D16Arb9*	18114539	-	18114756
16	*D16Wox10*	18121278	-	18121390
16	*D16Mgh9*	26915621	-	26915869
16	*D16Rat102*	34614773	-	34614907
16	*D16Rat19*	35339930	-	35340162
16	*D16Mgh5*	50266029	-	50266190
16	*D16Rat65*	61786275	-	61786423
16	*D16Rat53*	66606253	-	66606369
16	*D16Rat23*	69487513	-	69487718
16	*D16Rat14*	75400761	-	75400894
17	*D17Rat76*	13930241	-	13930458
17	*D17Rat8*	27619001	-	27619168
17	*D17Arb4*	40683664	-	40683905
18	*D18Rat62*	6934493	-	6934762

Table 2. Continued.

Chr	Marker	Position		
18	*D18Mit1*	12406975	-	12407219
18	*D18Rat137*	53987908	-	53988134
18	*D18Arb6*	58484894	-	58485101
19	*D19Rat28*	5035159	-	5035340
19	*D19Rat97*	9939385	-	9939600
19	*D19Rat11*	31605038	-	31605157
19	*D19Rat2*	55455213	-	55455363
20	*D20Rat46*	3040047	-	3040188
20	*D20Arb10*	52214730	-	52214999

Table 3. Primers used for the genetic mapping, mutation analysis, and quantitative RT-PCR (qPCR) in this study.

Experiment	Gene	Primer name	Primer sequence (5' - 3')	Position*	Expected product size (bp)	Template
Genetic mapping	*Cwf19l2*	Cwf19l2_MS_F	ACAGCTGCAGGACATAATGTTGACAG	437691-437655	168	Genomic DNA
		Cwf19l2_MS_R	AGAGCACTTGCCTAGCAAGCACAAG	437823-437798		
	Rbms2	Rbms2_MS_F	TTAGGTATATACAGAGTTATACTAAG	1467361-1467335	153	
		Rbms2_MS_R	AAACTACTTCACATGTCTGAAACC	1467538-1467514		
	Mip	Mip_MS_F	CAGGAAGATCCTAGGGCTCAG	1526124-1526145	322	
		Mip_MS_R	ATCTGCACATGTTCCCTTCC	1526446-1526426		
	Olf1060	Olf1060_MS_F	CCAAGTAACTGTACAAAGTACAAGCAT	7999887-7999913	155	
		Olf1060_MS_R	AGTAAATCTCATTAATACTAAGCAACCTG	8000042-8000014		
	Zfp347	Zfp347_MS_F	GTGTCTGAAGACAGCTACAATGTGTG	8877088-8877061	150	
		Zfp347_MS_R	CAACACTTTTCACCAAATACTGTTATG	8877238-8877212		
	Ankrd24	Ankrd24_MS_F	CCTGAAGTCACTCTGCTCATATACAC	9570803-9570776	149	
		Ankrd24_MS_R	ACATATCCACATCCTCAGGTGAAC	9570952-9570929		
Mutation analysis	*Mip*	Mip_F	TATTAGGGACCCAGGCACTGTGATTGC	1509031-1509057	5684	Genomic DNA
		Mip_R	TCCCCACAGTCTCTTTCTTCATCCAAGG	1514715-1514688		
		Mip_F1**	CTGTCCGAGGAAACCTAGCACTC	1509405-1509427		
		Mip_F2**	TTTCCTGGGAACTGGAC	1510119-1510135		
		Mip_F3**	TACGGGCTGTACAGAAG	1510829-1510845		
		Mip_F4**	TTCCCTGAAGAGTTCTG	1514494-1514510		
		Mip_R1**	GCAAAGATGCAGAGCAC	1510266-1510250		
		Mip_R2**	TGAGCAGGCATGTCAAG	1509476-1509460		
		Mip_del_F***	CTGTACAGTGTCACCCCACCAG	1509358-1509380	104 or 108	Genomic DNA
		Mip_del_R***	GTCAAGGCAACAGTCAGGACAC	1509483-1509461		
qRT-PCR	*Cryaa*	Cryaa_F	GTCATCTTCTTGGATGTGAAGCAC	226-249	118	cDNA
		Cryaa_R	GAAATGTAGCCATGGTCATCCTG	344-322		
	Crygb	Crygb_F	CAACACTCGGGCACTTACAGAATGA	283-307	177	
		Crygb_R	CCCTCTGTAGCTAGGCATCTCATAG	459-435		
	Crygd	Crygd_F	CAGACTGTACGAGAGGGAAGATTAC	312-336	102	
		Crygd_R	AGGGAGTAGATCTCATTGAAGTGG	413-390		
	Casp6	Casp6_F	AACCTGACTCGAAGGTTCTCAGAG	352-375	116	
		Casp6_R	GGAAGTCGACACCTCGTGAATCTT	453-430		
	Lim2	Lim2_F	TCATGACCTTCTTTGCAGGAATTTTC	488-513	115	
		Lim2_R	GTTGTAACTTCCGGCTGCAAGTTT	602-579		
	Bfsp1	Bfsp1_F	TGAGATTGAAGGCAACAGGTTGAGC	930-954	121	
		Bfsp1_R	CACAGCCCTGGTAAGATCTTTCACA	1050-1026		
	Bfsp2	Bfsp2_F	AGAGGTAGTCCATGTATCCCAGACC	962-988	148	
		Bfsp2_R	AAGGTGTTTTCCAGGCCTCGTTTCAG	1109-1083		
	Gja3	Gja3_F	GGTTGCCACCTTATTACACACAC	1022-1044	109	
		Gja3_R	TTTAGGGTCACCACTGTGAAGTC	1130-1108		
	Gja8	Gja8_F	GCTACCAGCTCCTAGAAGAAGAG	892-914	101	
		Gja8_R	AGACTCAAGGTATATTGGCACCAGC	1481-1457		

*Positions are according to the published *Mip* genomic sequence (Ensembl Gene ID: ENSRNOG00000003132), and *Cryaa* (NM_012534), *Crygb* (NM_001109875), *Crygd* (NM_033095), *Casp6* (NM_031775), *Lim2* (NM_053771), *Bfsp1* (NM_031555), *Bfsp2* (XM_003750577), *Gja3* (NM_024376), and *Gja8* (NM_153465) mRNA sequence.

**Primers used for sequencing

***Primers used for genotyping of *kfrs4* mutation

Watanabe. Figure 1

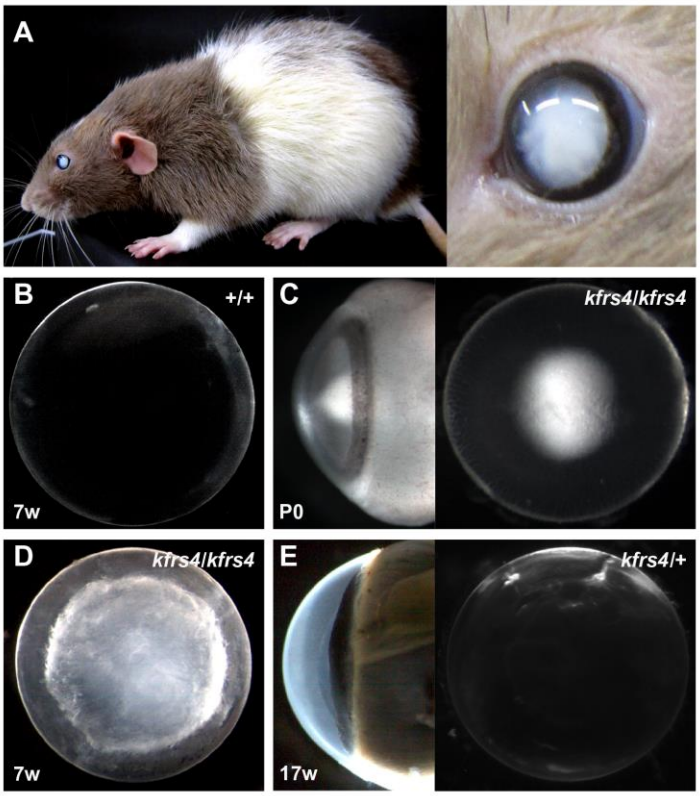

Watanabe. Figure 2

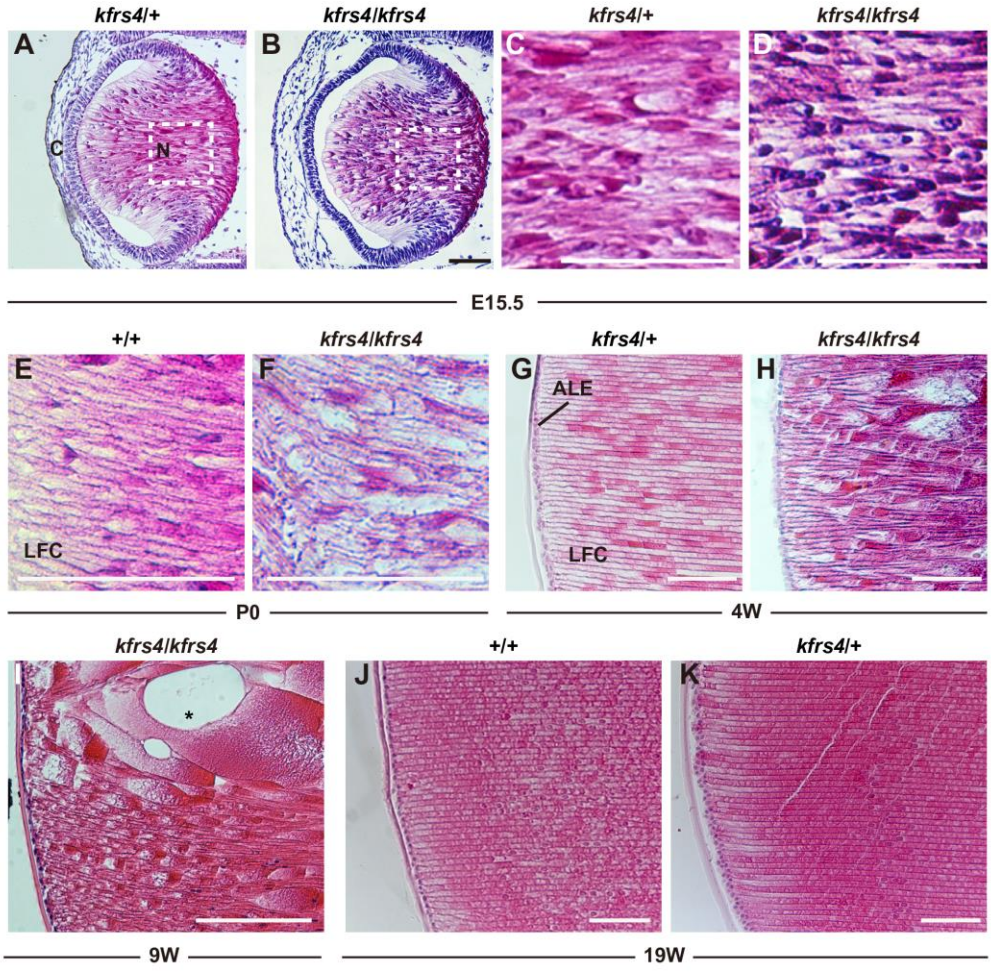

Watanabe. Figure 3

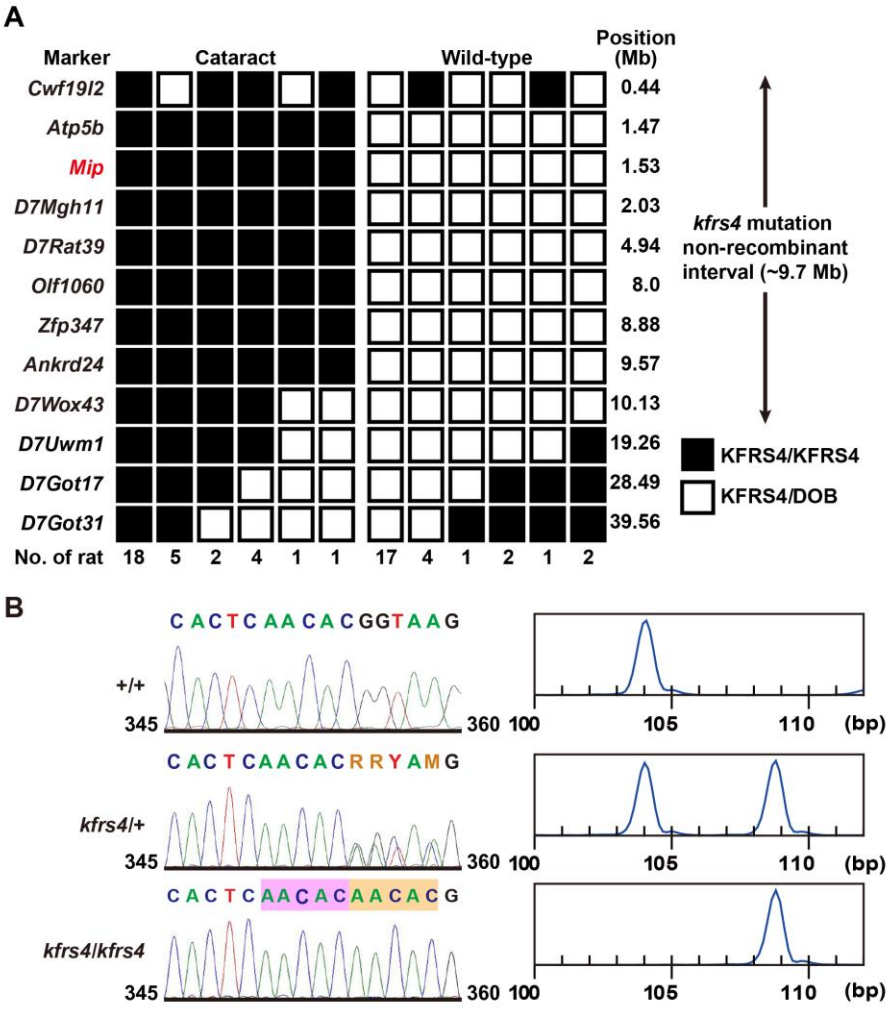

Watanabe. Figure 4

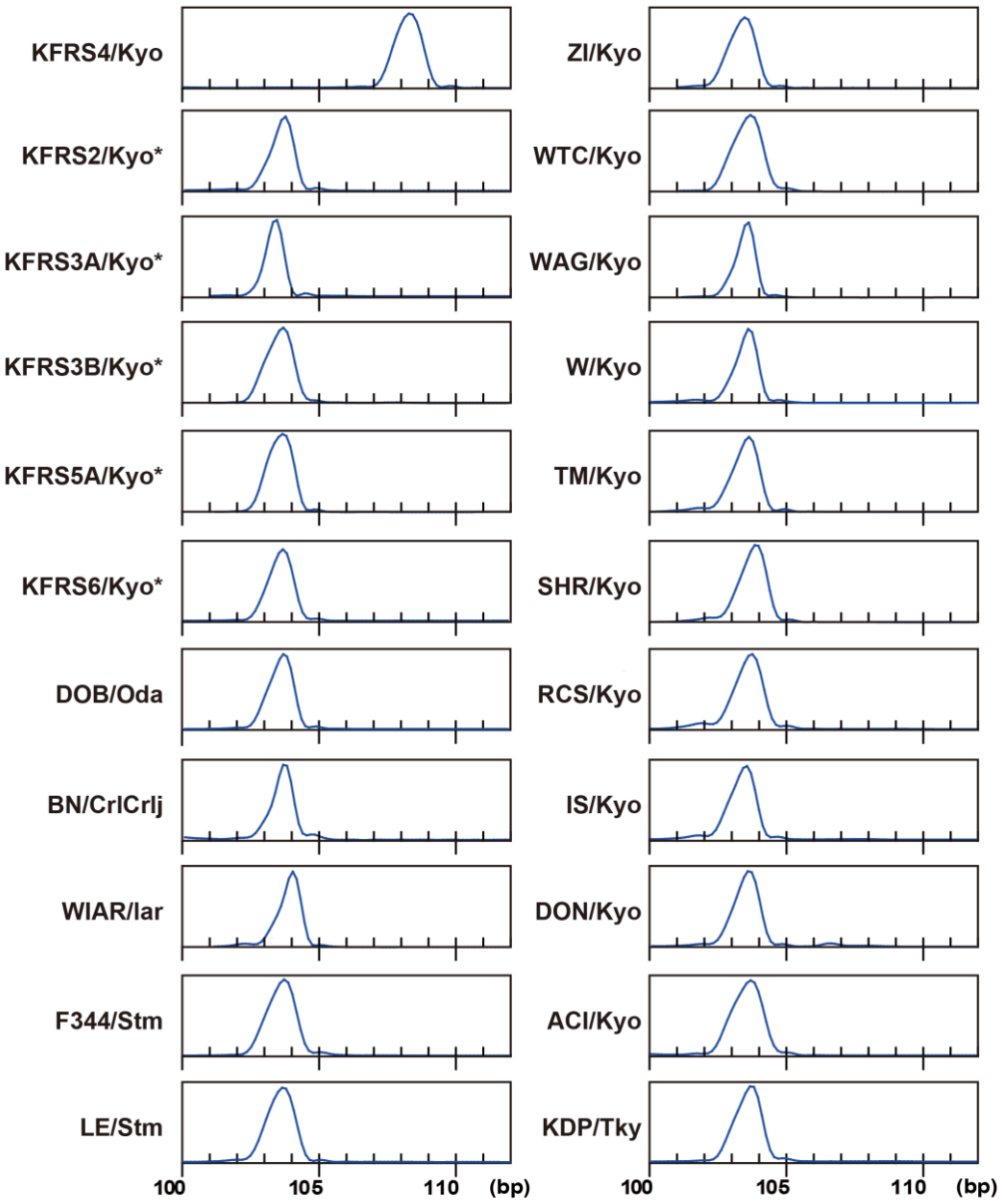

Watanabe. Figure 5

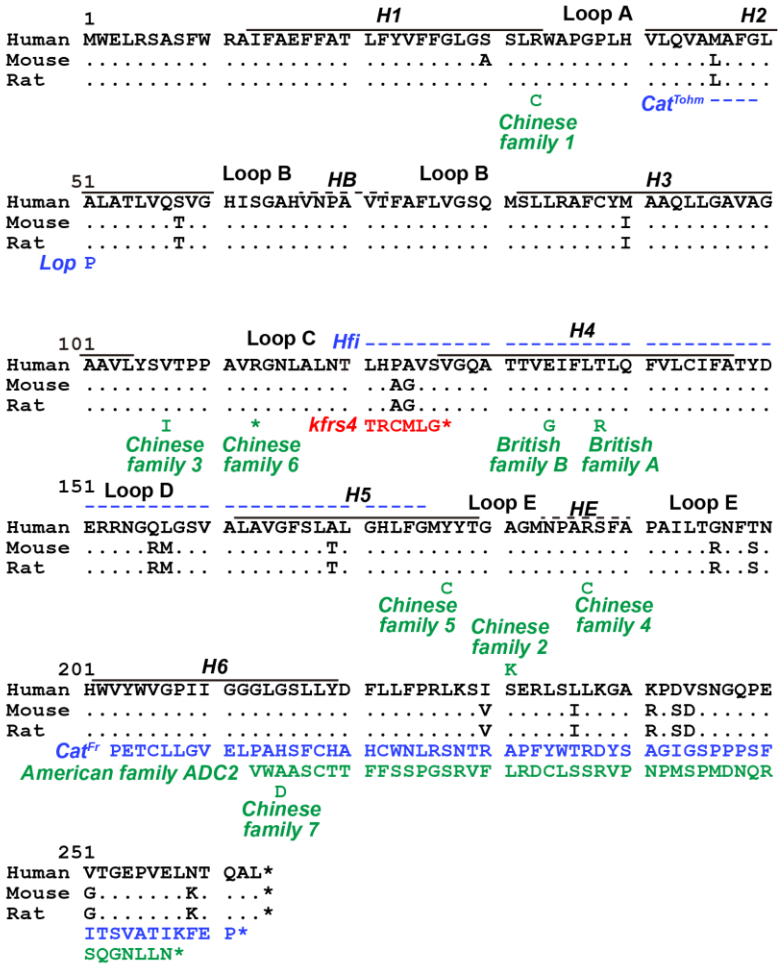

Watanabe. Figure 6

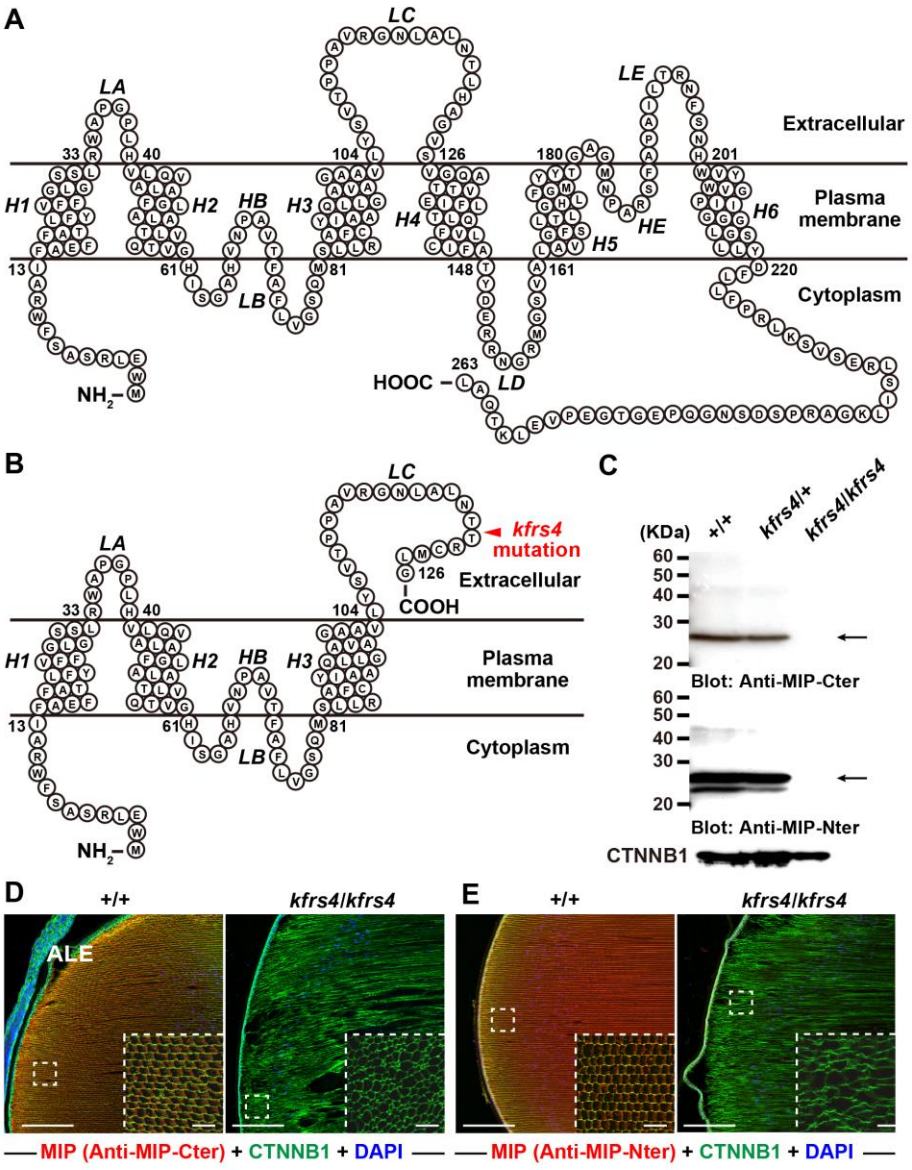

Watanabe. Figure 7

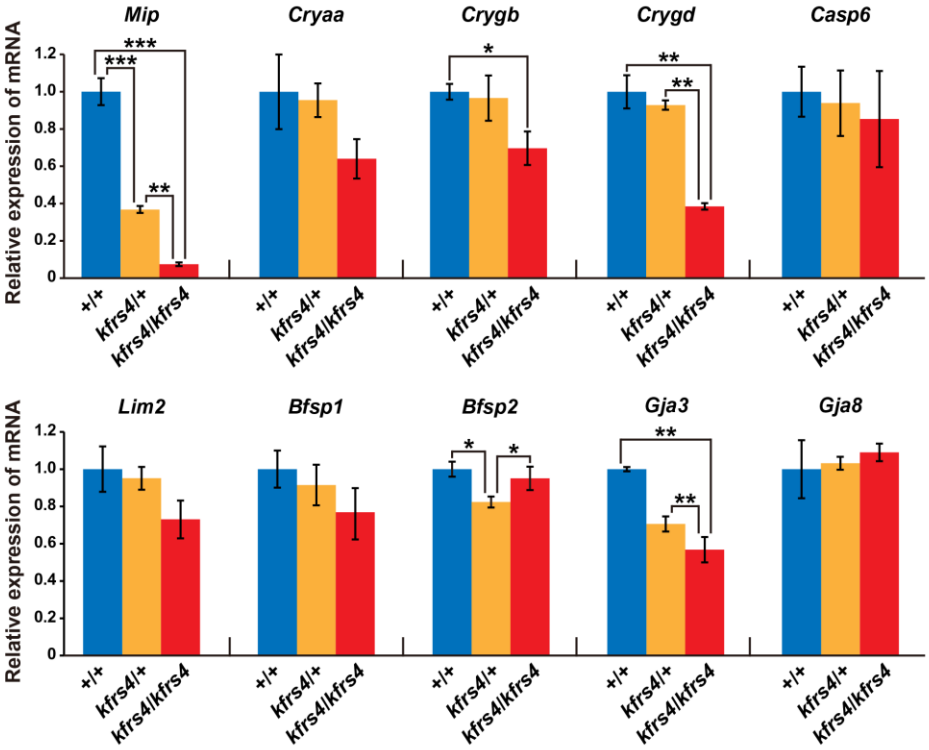

Watanabe. Figure 8

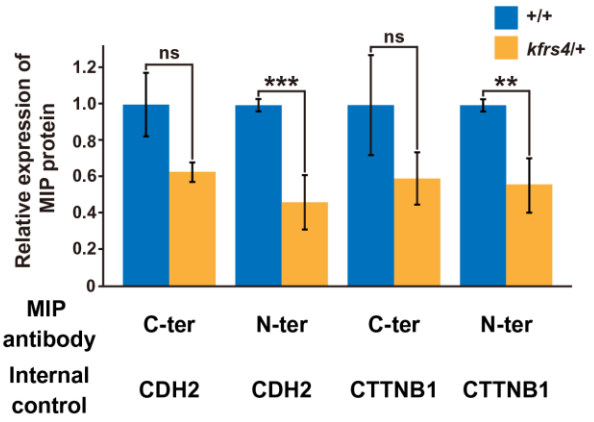

Watanabe. Figure 9